PRINT ISSN 1119-8362
Electronic ISSN 2659-1499

Full-text Available Online at
https://www.ajol.info/index.php/jasem
https://www.bioline.org.br/ja

J. Appl. Sci. Environ. Manage.
Vol. 29 (8) 2428-2434 August 2025

Effects of Thermal Expansion, Vertical Bending Loads, and Horizontal Braking Forces on Long-Span Continuously Welded Rail Systems in Emerging Railway Networks

[*1, 2]MAKAMA, RE; [2]BIN, Y; [1]ALFA, MI; [3]FIERKWAP, SB

[1]Department of Civil Engineering, University of Jos, Nigeria,
[2]School of Civil Engineering, Changsha, Central South University, China
[3]Department of Physics, University of Jos, Nigeria

**Corresponding Author Email: mrhishama2000@gmail.com*
ORCID: https://orcid.org/0009000037654081
Tel: +2348136322039

Other Author's Email: binyan@csu.edu.cn; meshilalfa@gmail.com; fierkwaps@unijos.edu.ng

ABSTRACT: The objective of this paper was to investigate the effects of thermal expansion, vertical bending loads, and horizontal braking forces on long-span continuously welded rail (CWR) systems in emerging railway networks using finite element modeling in SAP2000. Results obtained reveal that thermal loading generates critical compressive stress exceeding UIC 774-3R limits without expansion devices, while braking forces produce the highest tensile and compressive stresses (up to 10 MPa). Vertical loads, however, have negligible effects on rail integrity. The findings validate the effectiveness of expansion devices and emphasize the need for tailored design strategies for long-span bridges, providing practical insights for high-speed railway infrastructure in developing regions.

DOI : https://dx.doi.org/10.4314/jasem.v29i8.6

Cite this Article as: MAKAMA, R. E; BIN, Y; ALFA, M. I; FIERKWAP, S. B. (2025) Effects of Thermal Expansion, Vertical Bending Loads, and Horizontal Braking Forces on Long-Span Continuously Welded Rail Systems in Emerging Railway Networks. *J. Appl. Sci. Environ. Manage.* 29 (8) 2428-2434

Dates: Received: 30 May 2025; Revised: 21 June 2025; Accepted: 21 July 2025; Published: 01 August 2025

Keywords: Continuously welded rail; track-bridge interaction; thermal stress; braking forces; long-span bridges

The modernization and expansion of high-speed railway (HSR) systems around the world have significantly increased the engineering complexities associated with the design and maintenance of railway infrastructure. Among the critical issues is the phenomenon of Track-Bridge Interaction (TBI), which arises when continuously welded rail (CWR) is laid over bridge structures (Jian *et al*., 2020). CWR tracks are designed to eliminate joints over long stretches of railway line, thereby reducing maintenance costs and enabling smoother, faster, and more energy-efficient train operations ((Lim *et al*., 2003; Enshaeian and Rizzo, 2021). However, their monolithic nature also makes them sensitive to longitudinal displacements and internal forces generated from temperature variations, train braking or acceleration, and structural deformations of the bridge deck. Bridges with continuous spans are particularly prone to significant rail-structure interaction effects due to the cumulative axial forces and constraint conditions imposed at supports and bearings. Without proper mitigation measures, these interactions can result in excessive longitudinal stresses, loss of track alignment, and eventual structural or track failure (Wingler, 2018). International standards, such as the UIC Code 774-3R, have been developed to provide guidelines on allowable stress limits, the use of expansion devices,

**Corresponding Author Email: mrhishama2000@gmail.com*
ORCID: 0009000037654081
Tel: +2348136322039

and design requirements to mitigate these effects (UIC, 2001). In this context, finite element modeling (FEM) has emerged as a powerful tool to simulate and analyze the TBI phenomenon in various structural configurations. Previous research has demonstrated the application of FEM software such as ANSYS, MIDAS, and SAP2000 in assessing rail stress responses under thermal, vertical, and horizontal loads (Sowmiya *et al*., 2010; Shridhar, 2014). However, detailed studies focusing on the interaction behavior of CWR over long-span continuous girder beam bridges under combined loading conditions are still limited. TBI has been extensively studied in recent decades due to its significant implications on the stability and serviceability of railway infrastructure, especially with the introduction of high-speed and heavy-haul trains as stated earlier. Initial studies on TBI began with simplified analytical models that considered linear elastic behavior and uniform loading (Zhai *et al*., 2019). These models offered limited insights into real-world nonlinearities such as slip at fastener interfaces, temperature gradients, and support settlements. The evolution of computational capabilities led to the development of more complex numerical models using FEM. Xu *et al*. (2021) introduced a coupled train-track-bridge dynamic model, which simulated interaction forces under train movement and confirmed the importance of considering dynamic loads and boundary nonlinearities. CWR tracks are globally accepted for modern railways due to their ability to reduce impact loads and maintenance costs (Lim *et al*., 2003). However, the elimination of rail joints introduces challenges such as thermal expansion, which induces significant axial forces and displacements, particularly at bridge interfaces (Enshaeian and Rizzo, 2021). Studies by Lakušić (2012) and Šmalo and Ižvolt (2014) highlighted the sensitivity of CWR to temperature-induced stresses and the necessity of accommodating longitudinal movement through devices like expansion joints and sliding bearings.

Finite Element Analysis (FEA) has become the preferred method for analyzing TBI due to its ability to model nonlinear behaviors and complex boundary conditions. Jonex *et al*. (2023) presented a parametric study using ABAQUS to investigate the effect of fastener stiffness and rail pad properties on interaction forces. Sowmiya *et al*. (2010) used MIDAS Civil to simulate interaction forces under braking and acceleration scenarios and validated their model with field measurements. Despite the progress, most research focuses on short- to medium-span bridges or assumes idealized boundary conditions. A notable gap in literature regarding long-span continuous beam bridges with realistic assumptions exist, particularly in developing regions. This study addresses this gap by investigating the longitudinal stress distribution in rails laid on a (32.5 + 40 + 32.5) m continuous girder beam bridge using SAP2000. The paper evaluates the effects of temperature, bending, and braking loads on the axial stress in the rail with the aim of providing a practical reference for safe CWR track deployment on similar bridge types in emerging railway networks.

MATERIALS AND METHODS

This study employs a finite element modeling approach to simulate and analyze the interaction behavior between the continuous welded rail (CWR) track (see Fig. 1) and a continuous girder beam bridge using the SAP2000 software. The modeling focuses on a (32.5 + 40 + 32.5) m continuous bridge with rail laid across the superstructure and adjoining embankments. The methodology comprises model conceptualization, definition of material properties, boundary conditions, load application, and result extraction.

Fig. 1: A Continuously Welded Rail (CWR) Track (Source: Jones and Ashby, 2019).

Overview of track-bridge interaction modeling: Track-bridge interaction (TBI) modeling involves the coupling of two structural systems, the track and the bridge, subjected to various mechanical and environmental loads. Generally, the model must account for relative displacement between rail and deck (slip), resistance from fasteners and ballast (track-bed stiffness), boundary conditions at supports (fixed and movable), and axial stresses induced by temperature changes, vertical live loads, and horizontal braking/traction forces. SAP2000 was selected for its nonlinear link modeling capabilities, which enable a realistic simulation of the fastener behavior between the rail and bridge. Post-processing was carried out using Microsoft Excel for extracting and visualizing stress responses.

Model configuration and geometry: The modeled structure consists of a continuous three-span girder bridge with end spans of 32.5 m and a main span of 40 m, totaling 105 m. To simulate realistic boundary conditions, additional 100 m length of rail are modeled on both ends of the bridge to represent track laid on subgrade embankments, yielding a total system length of 305 m.

Coordinate System and Geometry: The coordinates were defined such that the X-axis represented the longitudinal rail/bridge direction X-axis, the Y-axis was the transverse direction, and the Z-direction represented the vertical direction. The span arrangement was set at 32.5 m + 40 m + 32.5 m (bridge) + 2 × 100 m (embankment rail). The rail and bridge deck were modeled using distinct materials with appropriate mechanical properties.

Material Properties: The rail (CHN60, 60 kg/m profile) and Bridge Deck (Concrete C50 grade, GB0010C50) properties and their respective values are indicated in Table 1.

Table 1: The rail (CHN60, 60 kg/m profile) and Bridge Deck (Concrete C50 grade, GB0010C50) properties and their respective values

Property	**The Rail**		**Bridge Deck**	
	Symbol	Value	Symbol	Value
Elastic modulus	E_r	2.0×10^5 MPa	E_c	3.45×10^4 MPa (based on C50 properties)
Poisson's ratio	v_r	0.3	v_c	0.2
Coef. of thermal expansion	α_r	1.2×10^{-5}/°C		
Density	ρ_r	7.85×10^{-6} N/mm³	ρ_c	2.5×10^{-6} N/mm³

Model building: The rail section was modeled as a line element with general cross-section defined in SAP2000 while the section properties were input to represent the CHN60 profile. The Bridge Section was modeled with variable-height box girders of 12 m constant width and varying height based on the following span position: *Mid-span*, the tallest section, as Section 1-1, *End-spans*, the shorter sections as Section 2-2, and *Supports*, which represent the transitional sections, as Section 6-6. Transitions between sections were created using *non-prismatic frames* of the SAP2000 software and designated as VAR1 to VAR4 to ensure geometric continuity. Fig. 2 shows the frame property window of the SAP2000 software.

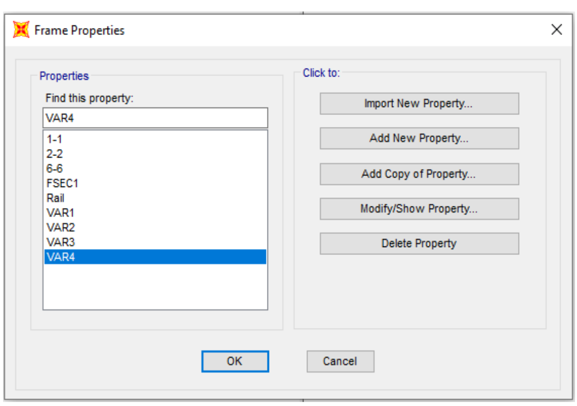

Fig. 2: The SAP2000 Window for Frame Properties

Boundary Conditions and Supports: Vertical stiffness was set at 60 MN/m and modeled using multilinear elastic link elements using the Link stiffness parameters, $k_{longitudinal}$ and $k_{vertical}$ derived from empirical fastener behavior (Sun *et al*., 2017). The boundary conditions and supports were modeled to replicate actual bridge conditions such that fixed support was fully restrained except rotation around the vertical axis (R3). Movable support was equally restrained in all directions except for vertical (U2) and longitudinal (R3) displacements. Rigid links were used to represent sleepers and distribute rail forces to bridge nodes. All supports were assigned appropriate rotational inertia (e.g., $I = 10^{14}$) to replicate stiffness effects accurately.

Loading Conditions: Three primary load conditions, thermal, flexural (vertical live load), and braking/traction, were applied to investigate TBI effects. For the thermal Load, a uniform temperature change of $\Delta T = 15$°C was applied to both bridge and rail to simulate summer thermal expansion. In the flexural scenario, a load of magnitude $\mathrm{q} = 64\mathrm{k\,N/m}$ (as specified by UIC and Chinese design code) was applied over five separate configurations (load on left end-span, load on left + middle spans, load on all spans, load on right + middle spans, and load on right end-span). For the braking/traction condition a horizontal load of $16\mathrm{k\,N/m}$ (assumed as 25% of vertical load) was applied over five conditions similar to the flexural load case to simulate braking effect from decelerating high-speed train. Fig. 3 depicts the continuous beam bridge model.

Meshing and Simulation: The beam was discretized into 1 m segments using SAP2000's node division tools to ensures fine resolution for capturing longitudinal stress gradients while the rail offset was placed at the top surface of deck to align centroid locations. Nonlinear static analysis was then used for all load cases ensuring that each load condition was run independently to isolate effects. The results were then extracted from SAP2000, filtered, and exported to Microsoft Excel where the axial stresses in the rail were plotted to assess tensile and compressive stress zones.

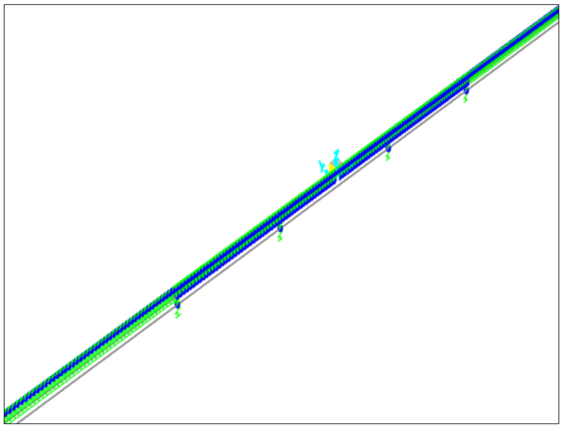

Fig. 3: 3D view of the continuous beam bridge model

Assumptions and Limitations: In this study we assumed that the lateral rail movement/dynamic effects are inconsequential, and fastener behaviour is modeled as bilinear elastic with no plastic slip. The Ballast-subgrade interaction is idealized as being uniform across the embankments. Although these assumptions simplify modeling, they are consistent with prior analytical frameworks (Jonex *et al*., 2023; UIC, 2001) and provide a conservative basis for evaluating stress distribution.

RESULTS AND DISCUSSION

This section presents the outcomes of the nonlinear finite element analyses conducted using SAP2000. The rail-bridge system was subjected to thermal loading, flexural (vertical) loading, and horizontal braking/traction forces. The analysis focused on the distribution and magnitude of longitudinal (axial) stresses induced in the rail under each loading condition, and the effectiveness of stress mitigation strategies such as expansion devices was evaluated. The graphical and tabulated data were exported to Microsoft Excel for interpretation.

Temperature load response: A uniform temperature of 15°C was applied to the rail-bridge system to simulate summer thermal expansion, with and without an expansion device at the bridge's right sliding bearing and the results are shown in Table 2. The rail experienced considerable axial stress concentrations near the sliding bearings, as shown in Fig. 4(a), which depicts the Axial stress of rail under temperature load without expansion adjuster. The peak compressive stress reached 89.05 MPa at the right sliding bearing, exceeding the UIC 774-3R code threshold of 72 MPa for compressive stress in CWR sections without adjusters (UIC, 2001). A tensile peak of 30.17 MPa occurred at mid-span under temperature load (with expansion adjuster). After introducing an expansion adjuster at the right bearing, the maximum compressive stress dropped significantly to 6.59 MPa, confirming the effectiveness of the device in mitigating thermal stress. Tensile stress remained similar at 30.58 MPa.

Again, from Fig. 4, the axial stress of the rail significantly drops when the expansion adjuster is set at the far-right end bearing of the continuous bridge. This causes a dip in the compressive stress at the far right bearing from an initial value of 110.065MPa to 6.739 MPa. The expansion device redistributes stress along the track and prevents localized overloading.

Flexural load response (vertical live load): The beam was subjected to a uniformly distributed vertical load of 64 kN/m, consistent with UIC and Chinese railway bridge design codes. The analysis was run for five separate loading configurations, and the result is presented in Table 3 and Fig. 5. From the results, tensile stresses peaked near the movable supports while the compressive stresses were generally observed at mid-span or load application points. All stress values remained below 2.5 MPa, indicating minimal TBI effect under bending alone. The relatively low magnitude of stresses confirms that vertical loads alone do not pose significant risk to axial rail integrity when the bridge and fasteners are well designed. This observation aligns with findings in Esveld (2001) and Sun *et al*. (2017), which noted that vertical loading effects on TBI are less critical than thermal or braking loads.

Table 2: Thermal load response with and without an expansion device at the bridge's right sliding bearing

Position	Without Expansion Device		With Expansion Device	
	Stress Type	Magnitude (MPa)	Stress Type	Magnitude (MPa)
Mid-span of bridge	Tensile	30.17	Tensile	30.58
Right sliding bearing	Compressive	89.05	Compressive	6.59
Left sliding bearing	Compressive	43.63	Compressive	43.53

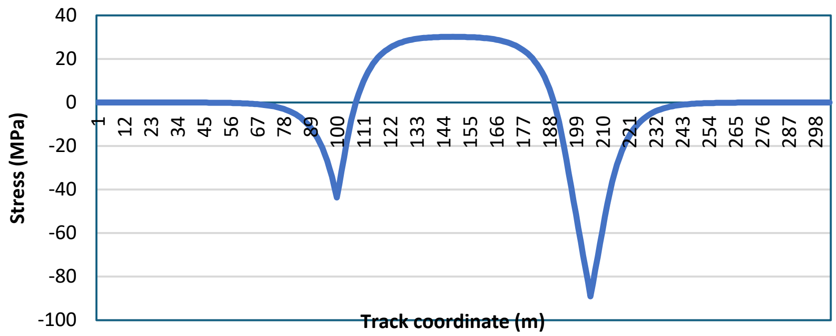

(a)

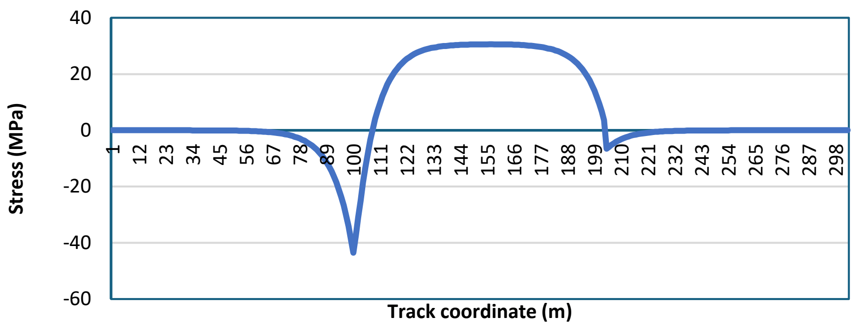

(b)

Fig. 4: Axial stress of rail under temperature load: (a) without expansion adjuster, (b) with expansion adjuster

Table 3*:* Flexural Load Response (Vertical Live Load) for different loading configurations

Load	Max. Compressive Stress (MPa)	Location (m)	Max. Tensile Stress (MPa)	Location (m)
Case 1	2.01	Left end-span (114)	2.35	Right embankment (204)
Case 2	1.51	Mid-Span (155)	1.30	Mid-Span (133)
Case 3	0.98	Mid-Span (193)	1.06	Mid-Span (133)
Case 4	1.94	Right end-Span (204)	1.72	Right embankment (100)
Case 5	1.54	Right end-Span (190)	1.84	Right embankment (204)

Table 4: Traction/braking effects simulated for 5 loading scenarios under the action of a breaking force

Load	Max. Tensile Stress (MPa)	Location (m)	Max. Compressive Stress (MPa)	Location (m)
Case 1	1.94	Left embankment (2)	8.06	Fixed support (133)
Case 2	1.94	Left embankment (2)	7.81	Mid-Span support (173)
Case 3	1.95	Left support (101)	9.84	Right support (204)
Case 4	9.15	Fixed support (133)	0.82	Right support (204)
Case 5	9.23	Mid-Span support (173)	–	Not recorded

In Case 1, with the load on the left end-span, the maximum compressive stress of 2.01 MPa occurs at 114 m, while the maximum tensile stress of 2.35 MPa appears at 204 m. Case 2 involves loading on the left end-span and mid-span, resulting in 1.51 MPa compressive stress at 155 m and 1.30 MPa tensile stress at 133 m. Case 3, with loads on both end-spans and the mid-span, yields the lowest stresses overall, with a compressive stress of 0.98 MPa at 193 m and tensile stress of 1.06 MPa at 133 m. In Case 4, where the load is on the right end-span and mid-span, compressive stress reaches 1.94 MPa at 204 m and tensile stress 1.72 MPa at 100 m. Lastly, Case 5, with loading on the right end-span alone, produces 1.54 MPa compressive stress at 190 m and 1.84 MPa tensile stress at 204 m. The results indicate that stress distribution is significantly influenced by the load position, with maximum tensile stresses typically occurring near the bridge's movable bearings.

Braking/traction load response (horizontal load): A distributed horizontal braking force of 16 kN/m was applied to represent traction/braking effects. Like the flexural load, five loading cases were evaluated, simulating varying braking zones from the left to right embankments. The results are presented in Table 4 and the schematic diagram shown in Fig. 6.

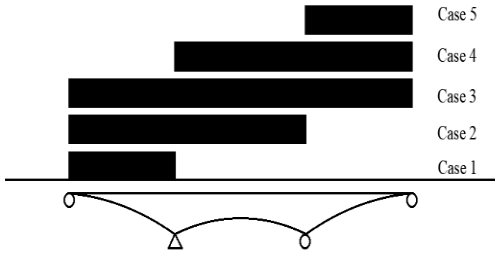

Fig. 5: Schematic diagram of the 5 working conditions under the action of bending force

Braking loads induced the highest axial rail stresses in the system, with compressive values peaking at 9.84 MPa and tensile stress reaching 9.23 MPa. While these values are within allowable limits for rail steel, they are notably higher than those generated by flexural loads. The spatial shift of peak stresses from left to mid-span supports with increasing brake zones demonstrates how braking direction and load placement influence rail stress distribution. This is consistent with modeling outcomes reported by Wingler (2018) and Mirković *et al.* (2017), emphasizing the need for careful assessment of braking zones in CWR design. The impact of a uniformly distributed braking load of 16 kN/m applied across five different loading scenarios on a continuous welded rail (CWR) bridge is investigated. Each case varies in the application span, ranging from embankments to mid-spans and end-spans. The result reveals that maximum compressive stresses occur near the supports and embankments, with the highest value of 9.84 MPa recorded in Case 3 at the right movable support**.** Tensile stresses, on the other hand, show a steady increase across the cases, reaching a peak of 9.23 MPa in Case 5 at the mid-span movable support. While tensile stress builds up progressively with increased loading coverage, compressive stress fluctuates, indicating a complex stress distribution response to braking loads. These results reinforce the UIC 774-3R recommendations, particularly the use of expansion adjusters and the strategic placement of fixed and movable supports. FEM proves effective in capturing these stress responses and can serve as a design validation tool for rail-bridge systems.

Overall analysis of the rail axial braking stress: The overall analysis of rail axial braking stress under five working conditions reveals distinct trends in the distribution and magnitude of both tensile and compressive stresses.

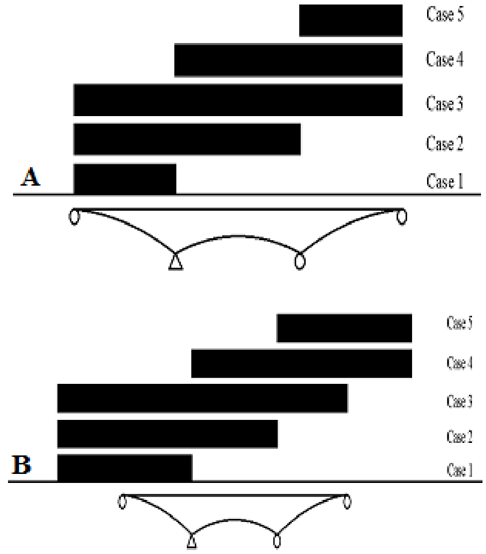

Fig. 6: Schematic diagram of the 5 working conditions under the action of: (a) bending force and (b) braking force

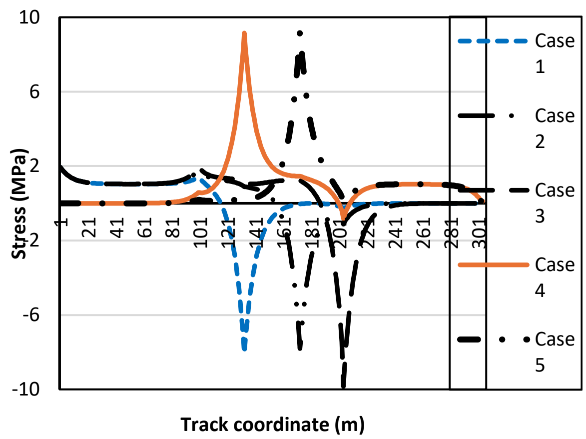

Fig. 7: Overall rail axial braking stress under five working conditions

As depicted in Fig. 7 and summarized in Tables 3 and 4, the maximum tensile stress occurs in Case 5, reaching 9.23 MPa at the mid-span movable support, with tensile stress values steadily increasing across the cases and shifting position from the left embankment toward the mid-span. In contrast, the maximum compressive stress of 9.84 MPa appears in Case 3 at the right movable support, showing a less consistent pattern—high in the first three cases but significantly reduced in the last two. The compressive stress locations also shift from the fixed support toward the right movable support, indicating a complex stress behavior influenced by varying braking load conditions.

Conclusion: This study performed a finite element analysis of track-beam interaction in a continuous welded rail system on a (32.5 + 40 + 32.5) m continuous girder bridge using SAP2000. The model considered thermal expansion, vertical loads, and braking forces, incorporating realistic boundary conditions and nonlinear rail decks. Thermal effects resulted in high compressive stresses that exceeded the allowable limits, but were reduced by the use of an expansion device. Vertical loads had minute impact on the rail stresses, while braking forces induced stress levels of up to 10 MPa. The analysis confirms temperature and braking to be the key factors in TBI behavior and highlights the value of nonlinear modeling in the bridge-track design.

Declaration of Conflict of Interest: The authors declare that no known conflict of interest or personal relationships that could have influence the work reported in this paper.

Declaration of Data Availability: Data are available upon request from the corresponding author.

REFERENCES

Enshaeian, A; Rizzo, P (2021). Stability of continuous welded rails: A state-of-the-art review structural modeling and nondestructive evaluation. Pro. Ins. Mech. Eng., Part F: *J. Rai. Rap. Tran.,* 235(10), 1291–1311. https://doi.org/10.1177/0954409720986661

Jones, DRH; Ashby, MF. (2019). Eng. Mat. 1. Elsevier. https://doi.org/10.1016/C2015-0-04446-X

Jonex, C; Taye, B; Moges, Z; Fikre, H (2023). Modeling and Analysis of Rail Pad Stiffness on Ballasted Railway Track.

Lakušić, S (2012). Track–bridge interaction on high-speed railways. In Roa. Rai. Inf. II: Pro. 2nd Int. Con. on Roa. Rai. Inf. (CETRA 2012), Dubrovnik, Croatia.

Lim, NH; Park, NH; Kang, YJ (2003). Stability of continuous welded rail track. *Comp. Stru.*, 81(22–23), 2219–2236. https://doi.org/10.1016/S0045-7949(03)00287-6

Lonsdale, CP (1999). Thermite rail welding: history, process developments, current practice and outlook for the 21st century. Pro. AREMA 1999 Ann. Conf., 1895(C), 18.

Mirković, N; Popović, Z; Vilotijević, M; Lazarević, L (2017). Track/bridge interaction – The aspect of bridge structure. *Buil. Mat. Stru.,* 60(1), 29–45.

Shridhar. A (2014). Estimation of Residual Stresses in Rail section using FEM. *Int. J. Eng. Res. Tech.,* 3(1), 1471–1478.

Šmalo, M; Ižvolt, L (2014). The possibility of the establishment of continuously welded rail track on the Tatra Electric *Railway. Trans. Pro.,* 9(4), 33–42. https://doi.org/10.21307/tp-2014-407

Sowmiya, LS; Shahu, JT; Gupta, KK (2010). Three Dimensional Finite Element Analysis of Railway Track. Publication SP – *Amer. Conc. Inst*., 95–115.

UIC (International Union of Railways). (2001). UIC Code 774-3R: Track/Bridge Interaction - Recommendations for Calculations (2nd ed.). Paris: UIC.

Wingler, DFA (2018). Fundamentals of Rail way - Track Engineering and Technology; Quotations for achieving sound and healthy Railway-Tracks of High-Quality fit for modern 'World-Class' Rail way- Service. 1–20.

Xu, L; Yu, Z; Shan, Z (2021). Numerical simulation for train–track–bridge dynamic interaction considering damage constitutive relation of concrete tracks. *Arch. Civ. Mech. Eng.,* 21(3), 116. https://doi.org/10.1007/s43452-021-00266-8

Zhai, W; Han, Z; Chen, Z; Ling, L; Zhu, S (2019). Train–track–bridge dynamic interaction: a state-of-the-art review. *Veh. Sys. Dyn*., 57(7), 984–1027. https://doi.org/10.1080/00423114.2019.1605085